https://doi.org/10.5194/egusphere-2026-4764
Preprint. Discussion started: 27 August 2026

Kinetic Partitioning with Effective Mass Accommodation for Secondary Organic Aerosol Simulations in Chemical Transport Modeling

Regina Luu[1], Meredith Schervish[1,a], Samuel E. O'Donnell[2], Jeffrey R. Pierce[2], and Manabu Shiraiwa[1,*]

1. Department of Chemistry, University of California, Irvine, CA, 92617, USA

2. Department of Atmospheric Science, Colorado State University, Fort Collins, CO, 80521, USA

a. now at Department of Veterinary Physiology and Pharmacology, Texas A&M University, College Station, TX, 77843, USA

* m.shiraiwa@uci.edu

Abstract

Secondary organic aerosols (SOA) can adopt liquid, amorphous semi-solid, or glassy solid states in the atmosphere. Previous model simulations have revealed that SOA adopt semisolid or glassy solid phase states over dry regions and in the upper troposphere. A highly viscous phase state in SOA particles can cause kinetic limitations in SOA partitioning, challenging traditional SOA treatments with equilibrium partitioning in chemical transport modeling. In this study, we develop a method to simulate kinetic partitioning of SOA accounting for the impacts of SOA phase state by utilizing effective mass accommodation coefficient (α_{eff}). We initially test this method in box modeling to calculate equilibration timescale of SOA partitioning for a wide parameter space for bulk diffusivity, volatility, and total aerosol mass loading. Comparison with the chemical timestep of 20 min in GEOS-Chem reveals that equilibrium partitioning is still applicable for particles with bulk diffusivity > 10^{-15} cm^2 s^{-1}, whereas kinetic partitioning is required for partitioning of semi- and low-volatile compounds into highly viscous particles. To reduce computational burden, we developed analytical equations with gas-particle mass transfer coefficient by effectively accounting for gas and bulk diffusion limitations. The application of the new α_{eff} kinetic partitioning scheme into GEOS-Chem predicts lowers SOA mass over drylands (e.g., Western US) in the boundary layer due to kinetically limited growth of viscous SOA particles, whereas SOA mass can be described well with equilibrium partitioning in most other areas at the surface and at 850 hPa. In the upper troposphere at 500 hPa, the α_{eff} -kinetic scheme predicts up to 50% higher

https://doi.org/10.5194/egusphere-2026-4764
Preprint. Discussion started: 27 August 2026

SOA mass as evaporation is suppressed for glassy particles. The developed method is easily applicable, improving description and treatments of SOA in chemical transport models.

Short summary: The occurrence of semisolid and glassy phase states in SOA challenges traditional model treatments of equilibrium partitioning of SOA. We developed an effective method to treat kinetic partitioning of SOA by resolving the effects of particle phase state in chemical transport modeling. The application in GEOS-Chem reveals that SOA budget is impacted significantly especially over drylands and in the upper troposphere.

1 Introduction

Secondary organic aerosols (SOA) are ubiquitous and represent a major fraction of the submicron particulate matter in the troposphere, playing a central role in aerosol effects on climate, air quality, and public health (Jimenez et al., 2009; Pöschl & Shiraiwa, 2015; Shrivastava et al., 2017). Unlike primary organic aerosols which are directly emitted into the atmosphere, SOA are formed in the atmosphere from oxidation of biogenic or anthropogenic volatile organic compounds (VOCs) into lower-volatility products that may nucleate or condense onto pre-existing particles (Hallquist et al., 2009; Kirkby et al., 2023; Kroll & Seinfeld, 2008). SOA formation has been extensively studied in laboratory experiments, but there is still significant gap between ambient measurements and model simulations of SOA concentrations and properties by chemical transport models (CTMs) (Hallquist et al., 2009; Hodzic et al., 2016; Tsigaridis et al., 2014).

An important physical property of SOA particles is particle phase state which can vary from liquid (characterized by dynamic viscosity $\eta < 10^2$ Pa s), semisolid ($10^2 < \eta \leq 10^{12}$ Pa s), to glassy solid states ($\eta > 10^{12}$ Pa s) depending on the chemical composition, temperature, and relative humidity (Koop et al., 2011; Reid et al., 2018; Virtanen et al., 2010). Traditionally, SOA particles are assumed implicitly to be liquid-like in CTMs (Chung & Seinfeld, 2002; Pye & Seinfeld, 2010). The assumption holds that the gas-particle equilibration timescale is rapid in comparison to other atmospheric processes implying that SOA particles achieve instantaneous equilibrium partitioning between the gas and particle phases (Pankow, 2003). However, there has been mounting evidence of laboratory measurements and ambient observations showing that SOA can exist in glassy solid

https://doi.org/10.5194/egusphere-2026-4764
Preprint. Discussion started: 27 August 2026

or amorphous semisolid states as influenced by chemical composition and ambient conditions (Jensen et al., 2025; O'Brien et al., 2014; Saukko et al., 2012; Vaden et al., 2011; Virtanen et al., 2010).. A highly viscous phase state can lead to prolonged equilibration timescales of SOA partitioning, depending on volatility of species and particle mass loadings (Li & Shiraiwa, 2019; Schervish et al., 2024). We have developed methods to predict SOA phase state and viscosity (DeRieux et al., 2018; Li et al., 2020; Shiraiwa et al., 2017); their applications in CTMs suggest that SOA particles should adopt a viscous phase state over drylands and in the free troposphere (Luu et al., 2025; Schmedding et al., 2020; Shiraiwa et al., 2017; Zhang et al., 2024). The major limitation with most SOA phase state modeling studies is that the phase state prediction was applied as offline and post-processing calculations, while there are several studies explicitly resolving kinetic SOA partitioning (He et al., 2025; Shrivastava et al., 2024).

Implementing kinetic partitioning with explicit consideration of the effect of SOA phase state is essential in CTMs to improve SOA budgets and thereby aerosol impacts on air quality, climate, and public health. Process-level microphysics models such as the kinetic multi-layer model of gas-particle interactions in aerosols and clouds (KM-GAP) (Shiraiwa et al., 2012) can resolve kinetic limitations imparted by semi-solid or glassy solid phase states, but applying the same methodology to a CTM would drastically increase computational costs. Therefore, in this work, we develop a model scheme for the partitioning of organic compounds that is modulated by online calculations of SOA phase state by utilizing an effective mass accommodation coefficient (Shiraiwa & Pöschl, 2021). We investigate the influence of particle phase state, volatility, and total organic aerosol concentration on gas-particle partitioning of organic compounds in SOA. Then, we implement our partitioning scheme into the global CTM, GEOS-Chem, to evaluate the impacts of SOA phase state on SOA budgets.

2 Methods

2.1 Validation of partitioning method with a box model

Based on absorptive partitioning theory (Pankow, 1994), the mass transfer rates between gas and particle phases can be expressed for gas- (C^g) and particle-phase (C^p) mass concentrations (in µg m^{-3}) of semi-volatile compounds with the following ordinary differential equations (Shiraiwa & Pöschl, 2021; Trump et al., 2014):

https://doi.org/10.5194/egusphere-2026-4764
Preprint. Discussion started: 27 August 2026

$$\frac{dC^{g}}{dt} = -k_{gp}\left(C^{g} - \frac{C^{p}}{C_{OA}}C^{0}\right) \quad (1)$$

$$\frac{dC^{p}}{dt} = k_{gp}\left(C^{g} - \frac{C^{p}}{C_{OA}}C^{0}\right) \quad (2)$$

Partitioning is also dependent on the ratio of particle-phase concentration, C^{p}, and C_{OA} (μg m^{-3}), the total organic aerosol concentration. C^{0} (μg m^{-3}) is the temperature-dependent equilibrium vapor concentration and is described via the Clausius-Clapeyron relation:

$$C^{0}(T) = C^{0}(298\ \mathrm{K})\exp\left(\frac{\Delta H_{vap}}{R}\left(\frac{1}{298\ \mathrm{K}} - \frac{1}{T}\right)\right) \quad (3)$$

where R is the molar gas constant in J mol^{-1} K^{-1} and T refers to the ambient temperature in K. Species with a low volatility tend to have a higher enthalpy of vaporization, ΔH_{vap} (kJ mol^{-1}), as described by the semi-empirical parameterization (Stolzenburg et al., 2018; Stolzenburg et al., 2022):

$$\Delta H_{vap} = -5.7 \times \log_{10} C^{0}(298\ \mathrm{K}) + 129 \quad (4)$$

k_{gp} (s^{-1}) is the first-order gas-particle mass transfer coefficient or otherwise termed as a condensation sink, which we approximate by assuming a monodisperse aerosol population:

$$k_{gp}(\beta) = 2\pi D_{g} D_{p} N_{p} \beta \quad (5)$$

$$\beta(Kn, \alpha_{eff}) = \frac{0.75\alpha_{eff}(1 + Kn)}{Kn^{2} + Kn + 0.283Kn\alpha_{eff} + 0.75\alpha_{eff}} \quad (6)$$

Where D_{g} (cm^{2} s^{-1}) is the gas-phase diffusivity and D_{p} (cm) is the particle diameter. The term β is the Fuchs-Sutugin correction factor for gas diffusion in the transition regime, which is a function of the Knudsen number (Kn) and the effective mass accommodation coefficient (α_{eff}). Kn is the ratio of the mean free path in the gas phase (λ) as calculated using the mean thermal velocity (ω), and D_{p}: $Kn = 2\lambda / D_{p} = 6\ D_{g} / (\omega\ D_{p})$ (Pöschl et al., 2007). We assume a monodisperse particle population initialized at D_{p} = 100 nm with particle growth/loss considered only through condensation/evaporation as the number concentration is held constant while C_{OA} may vary.

https://doi.org/10.5194/egusphere-2026-4764
Preprint. Discussion started: 27 August 2026

α_{eff} describes the probability of a gas molecule colliding with a particle surface to enter the condensed phase, considering potential kinetic limitation of bulk diffusion in the particle phase as described as follows (Shiraiwa & Pöschl, 2021):

$$\alpha_{\text{eff}} = \alpha_{\text{s}} \frac{1}{1 + \frac{\alpha_{\text{s}} \omega C^0}{4 D_{\text{b}} \rho_{\text{p}}} \frac{D_{\text{p}}}{10} \times 10^{-12}} \tag{7}$$

where α_{s} is the surface accommodation coefficient, which is assumed to be 1 (Julin et al., 2014), and ρ_{p} (g cm^{-3}) is the particle density. Note that most studies assume certain fixed values for mass accommodation coefficient (often 1, 0.5, or 0.1) without considering the effect of particle phase state (Zaveri et al., 2020). α_{eff} provides an efficient way of accounting for the influence of species volatility and bulk diffusivity, D_{b} (cm^2 s^{-1}) on SOA partitioning (Shiraiwa & Pöschl, 2021). The conversion factor 10^{-12} allows volatility to be inserted in the commonly used μg m^{-3} units. The application of α_{eff} in traditional mass transfer equations yielded consistent simulation results with a kinetic multilayer model (KM-GAP) and two-film model (MOSAIC) (Zaveri et al., 2014) and α_{eff} successfully explained experimentally measured accommodation coefficient in SOA partitioning (Liu et al., 2019; Shiraiwa & Pöschl, 2021).

To solve the stiff ODE system of Eqs. (1) and (2), we use the Livermore Solver for Ordinary Differential Equations (LSODE) in double precision (DLSODE) (Hindmarsh, 1983). The use of an ODE solver can be computationally expensive especially when implemented in a CTM; therefore, we also treat Eq. (1) with an exponential approximation accompanied with the assumption that the equilibrium concentration is known *a priori*. The derivation of this approximation is as follows: at equilibrium, the net mass transfer rate between the gas and particle phase is zero.

$$\frac{dC^{\text{g}}}{dt} = 0 \tag{9}$$

Substituting Eq. (1) into Eq. (9) gives the following equation knowing that the condensation sink cannot be zero.

$$\frac{C^{\text{p}}}{C_{\text{OA}}} C^0 = C^{\text{g}}_{\text{eq}} \tag{10}$$

https://doi.org/10.5194/egusphere-2026-4764
Preprint. Discussion started: 27 August 2026

At equilibrium, the gas-phase concentration would be the product of the particle-phase mass fraction of a species and its volatility. Substitution of Eq. (10) into Eq. (1) gives:

$$\frac{dC^{g}}{dt} = -k_{gp}\left(C^{g} - C^{g}_{eq}\right) \tag{11}$$

Eq. (11) can be solved analytically with integration by separation of variables to obtain the following analytical solution of the gas-phase concentration at time, t, when initial and equilibrium concentrations are known as well as the condensation sink of that species.

$$C^{g}(t) = C^{g}_{0} - \left(C^{g}_{0} - C^{g}_{eq}\right)\left(1 - e^{-k_{gp}t}\right) \tag{12}$$

We conducted model simulations of SOA partitioning using a standalone zero-dimensional box model to calculate and compare two timescales of SOA partitioning, equilibration and mixing timescales, under various environmental conditions and mass loadings. The *e*-folding timescale to achieve gas-particle equilibrium or otherwise known as the equilibration timescale, τ_{eq} is calculated for the first instance (t) when the following inequality is satisfied (Li & Shiraiwa, 2019):

$$\frac{\left|C_{p}(t) - C_{p,eq}\right|}{\left|C_{p,0} - C_{p,eq}\right|} < \frac{1}{e} \tag{13}$$

$C_{p,0}$ and $C_{p,eq}$ refer to the initial and equilibrium mass concentration of a diffusing compound in the particle phase, respectively. τ_{eq} of a partitioning species also corresponds to approximately the inverse of its $k_{gp,}$ given that k_{gp} is held constant. We simulated partitioning under a closed system in which condensation of a species depletes its gas-phase mass concentration (C_g) while the particle-phase mass concentration increases (C_p) whereas the opposite occurs under evaporation conditions. A closed system configuration is best suited for integration into the GEOS-Chem partitioning module as partitioning occurs within a chemical time step where the gas phase is not replenished.

For the evaluation of kinetic limitations of bulk diffusion in a single particle, the characteristic mixing timescale, τ_{mix}, can be calculated as (Seinfeld & Pandis, 2016; Shiraiwa et al., 2011):

$$\tau_{mix} = \frac{D_{p}^{2}}{4\pi^{2}D_{b}} \tag{14}$$

https://doi.org/10.5194/egusphere-2026-4764
Preprint. Discussion started: 27 August 2026

where D_p is particle diameter which is assumed to be 100 nm and τ_{mix} is the timescale for a diffusing molecule to diffuse and establish a uniform concentration within the particle (Li & Shiraiwa, 2019). Note that τ_{eq} is fundamentally different from τ_{mix}, as a homogeneously mixed bulk phase is not a necessary requirement to achieve gas-particle partitioning equilibrium. Additionally, while τ_{mix} is solely determined by D_b and particle diameter, τ_{eq} is also affected by gas diffusion, volatility and absorptive mass concentration (Li & Shiraiwa, 2019; Maclean et al., 2017; Schervish & Shiraiwa, 2023; Shiraiwa et al., 2012). Comparison of the two timescales with regards to modeling partitioning is explored in Sect. 3.1.

The box model was designed to emulate all the relevant processes used in the standard GEOS-Chem complex scheme partitioning. Temperature, C^0(298K), particle D_b, and initial concentrations of the gas- and particle-phase species are all prescribed for the box model simulations. A non-volatile particle-phase species is used to establish initial background aerosol $C_{OA.}$ The volatilities of all species are temperature-corrected using Eq. (3) and (4).

2.2 GEOS-Chem Global Model Set up

We used the global chemical transport model, GEOS-Chem (ver. 14.1.1) to simulate organic aerosols in the troposphere (Community, 2024b; Lin et al., 2024). The model system was used to simulate the atmospheric composition in the year 2020 with a horizontal grid resolution of 4°x5° and 47 vertical layers extending to about 80 km altitude (0.1 hPa) using terrain-following (sigma) coordinates near the surface. The model spin-up was six months, after which the following 12-month outputs were recorded and analyzed. The recommended timesteps for this model resolution are 10 min for transport and 20 min for chemistry. Details on the meteorology and emission inventories used are the same as in our previous study, Luu et al., 2025.

The full chemistry mechanism with the complex SOA scheme including semi-volatile POA was applied. In this scheme, all SOA components are represented by a volatility-basis set (VBS) based on Pye et al. (2010)(Pye et al., 2010) apart from isoprene SOA (ISOA) and organo-nitrate SOA, which are modeled through a reactive uptake scheme (Fisher et al., 2016; Marais et al., 2016). Thus, ISOA, excluded from the VBS bins, are also excluded from contributing to the absorbing SOA mass for partitioning purposes, while we do include ISOA for particle phase state calculations. D_b is calculated based on assigned glass transition temperature (T_g) values, temperature, relative humidity, and particle mass concentrations. Assigned T_g values were based on our previous study

https://doi.org/10.5194/egusphere-2026-4764
Preprint. Discussion started: 27 August 2026

(Luu et al., 2025). Briefly, T_g of SOA component in each volatility bin ($T_{g,i}$) is calculated based on each component's volatility and oxygen-to-carbon (O:C) ratio (Table S1) (Li et al., 2020):

$$T_{g,i} = 289.10 - 16.50 \times \log_{10}(C^0) - 0.29 \times \left[[\log_{10}(C^0)]^2 + 3.23 \times \log_{10}(C^0)\,(O{:}C)\right] \quad (8)$$

T_g of dry SOA is calculated considering mass fraction of each component and T_g of SOA at ambient RH is calculated considering water uptake using the Gordon-Taylor equation. Using the modified Vogel-Fulcher-Tammann (VFT) equation, T_g, is converted to particle viscosity, which is then converted to D_b with the fractional Stokes-Einstein equation. The detailed steps including key equations and parameters can be found in our previous studies (Li et al., 2020; Luu et al., 2025; Shiraiwa et al., 2017).

For the current work, only reversibly partitioning species are modified which includes the oxidation products of monoterpenes and sesquiterpenes (TSOA) and oxidation products of light aromatics (ASOA) and intermediate volatility organic compounds (IVOCs). The VBS for TSOA covers C^0 of 0.1, 1, 10, and 100 μg m^{-3}, while ASOA uses C^0 of 10^{-10}, 1, 10, and 100 μg m^{-3} (Community, 2024a). In addition, we updated the heat of vaporization, previously assumed as 42 kJ mol^{-1} for all organic species, to be temperature and volatility dependent using Eq. (4) (Pye et al., 2010; Pye & Seinfeld, 2010). To maintain consistency with our previous methodology (Luu et al., 2025), we adjusted the molecular weights of all SOA components based on molecular corridors (Shiraiwa et al., 2014), as shown in Table S1.

While the aforementioned kinetic theory behind gas-particle partitioning has been applied in process-level modeling, large-scale transport models such as GEOS-Chem primarily rely on a thermodynamic partitioning method known as absorptive partitioning theory (Chung & Seinfeld, 2002). An alternative configuration for GEOS-Chem coupled with an online aerosol microphysics module (TOMAS) does not utilize thermodynamic partitioning as SOA is treated as non-volatile. GEOS-Chem-TOMAS, however, portions SOA based on effective surface area with the $\alpha = 1$ assumption (D'Andrea et al., 2013; Pierce & Adams, 2009). The details of absorptive partitioning method solving for the equilibrium gas and particle concentration values via a root finding algorithm is further explained in Chung & Seinfeld, (2002). This necessitates that chemical equilibrium is reached within the model's chemical time step (Kanakidou et al., 2005). This assumption is, however, not always true, especially when the particle phase state is highly viscous.

https://doi.org/10.5194/egusphere-2026-4764
Preprint. Discussion started: 27 August 2026

Thus, we use α_{eff} to account for these kinetic limitations to SOA partitioning with an assumption of particle diameter of 100 nm.

Composition-dependent D_b is used to determine which algorithm the gas-particle partitioning proceeds through: (1) default GEOS-Chem instantaneous equilibrium or the (2) analytical solution as elaborated on in Sect. 3.1. If the analytical solution is selected, the condensation sink is calculated as shown in Eq. (5, 6) using α_{eff} and Eq. (12) is used to determine final gas and particle concentrations at the end of the chemical time step.

3 Results and Discussion

We first show the box model results of six representative cases to illustrate how different partitioning treatments of the condensing species affect the time evolution of its gas-phase and particle-phase concentrations. Then we show GEOS-Chem results on the impact of the updated partitioning scheme on simulated global SOA budgets.

3.1 Zero-dimensional Box Model Simulations

Figure 1 shows the exemplary simulation results for the partitioning of a semi-volatile species of either a C^0 = 0.1 μg m^{-3}(a, d), 10 μg m^{-3} (b, e), or 100 μg m^{-3} (c, f). The initial seed concentration is assumed to be 10 μg m^{-3} with a number concentration of 1×10^4 cm^{-3}, representative of polluted conditions, and the initial particle diameter is 100 nm. Initial mass concentrations of semi-volatile species in the gas and particle phases are set to 0.1 and 0 μg m^{-3}, respectively. Two D_b cases are tested for the particle phase: $D_b = 10^{-11}$ cm^2 s^{-1} (a, b, c) or 10^{-18} cm^2 s^{-1} in (d, e, f)**.** Per case, three simulations are shown where the treatment of partitioning differs: (1) by solving the system of ODEs numerically, Eq. (1 and 2) with α_{eff}, (2) by solving the analytical solution, Eq. (12), or (3) same as method (1) except with the assumption of perfect mass accommodation (α = 1). An internal time stepping loop is used to iteratively recalculate the condensation sink for both the numerical and analytical solutions.

For partitioning into liquid particles (Fig. 1a-c), particle-phase concentrations reach equilibrium concentrations rapidly with τ_{eq} of ~10^2 s, equivalent to the condensation sink timescale set by gas-phase diffusion, indicating little kinetic limitations of bulk diffusion and a well-mixed particle bulk with τ_{mix} of ~0.03 s. Note that τ_{eq} is longer than τ_{mix} as the partitioning is governed by gas-phase diffusion and the condensation sink rather than D_b. The numerical solutions whether

https://doi.org/10.5194/egusphere-2026-4764
Preprint. Discussion started: 27 August 2026

using α_{eff} (black lines) or $\alpha = 1$ (red dotted lines) give identical results as α_{eff} is almost 1 with high D_b. The analytical solution (blue dashed lines) also yields practically identical results. Figure 1 d-f present simulations for highly viscous particles ($D_b = 10^{-18}$ cm^2 s^{-1}) with τ_{mix} of ~2×10^6 s, showing that partitioning proceeds with much longer equilibration timescales ($\tau_{eq} > 10^4$ s) due to strong kinetic limitations of bulk diffusion. The simulations with $\alpha = 1$ (red dotted lines) overestimates partitioning rates substantially. For the partitioning of low volatility species with $C^0 = 0.1$ µg m^{-3} (Fig. 1d), τ_{eq} is shorter at ~10^4 s as partitioning occurs relatively quicker due to low volatility nature of the condensing species rapidly establishing a local equilibrium between the gas phase and the near-surface bulk (Li & Shiraiwa, 2019). With higher volatility ($C^0 = 10$ and 100 µg m^{-3} in Fig. 1e and f, respectively), τ_{eq} becomes longer as re-evaporation becomes relevant due to their semi-volatile nature. However, in this case τ_{mix} overestimates τ_{eq} as partitioning is finished before a well-mixed bulk is established; the use of τ_{mix} to represent partitioning timescale would lead to significant underestimation of SOA mass. This further exemplifies how the two timescales cannot be interchangeable as they are physically distinct. For all cases represented in Fig. 1, both the numerical and analytical solutions are identical in simulating particle growth. Overall, τ_{eq} can be longer than the CTM chemical timestep of 20 min under a multitude of ambient conditions, indicating that proper consideration of kinetic limitations of bulk diffusion is required.

https://doi.org/10.5194/egusphere-2026-4764
Preprint. Discussion started: 27 August 2026

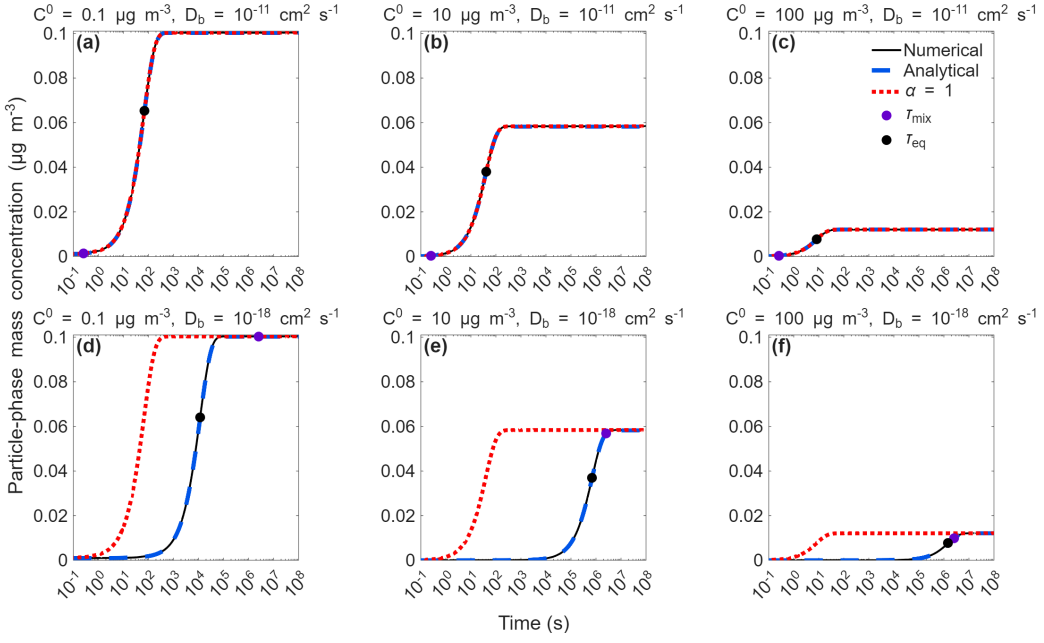

Figure 1. Temporal evolution of partitioning of semi-volatile species with C^0 = 0.1 μg m^{-3} **(a, d)**, C^0 = 10 μg m^{-3} **(b, e)**, or C^0 = 100 μg m^{-3} **(c, f)** into seed particles with initial concentrations of 10 μg m^{-3} with D_b = 10^{-11} cm^2 s^{-1} in **(a-c)** or D_b = 10^{-18} cm^2 s^{-1} in **(d-f)**. The temperature was set to 298 K, and the initial particle diameter was 100 nm. τ_{mix} and τ_{eq} are marked by purple and green dots, respectively.

To further probe the parameter space for kinetic partitioning, we computed contour plots of τ_{eq} as a function of D_b, C^0, and C_{OA} of 0.1 μg m^{-3}, 1 μg m^{-3} and 10 μg m^{-3}. Figure 2 shows the contour plots of τ_{eq} as calculated using the numerical solution. Note that the simulations were also conducted for evaporation, yielding very similar timescales and the results of Fig. 2 are directly applicable to evaporation (Shiraiwa & Seinfeld, 2012; Shiraiwa et al., 2013). In the low bulk diffusivity (D_b < 10^{-15} cm^2 s^{-1}) regime, τ_{eq} becomes prolonged with lower D_b due to kinetic limitations of bulk diffusion, while τ_{eq} shortens for lower C^0 as partitioning becomes largely determined by the condensation sink as there is efficient condensation with very slow re-evaporation of lower volatility compounds (Li & Shiraiwa, 2019). τ_{eq} is shorter for higher C_{OA} due to higher condensation sink, while this dependence is weaker compared to D_b and C^0. With an increased mass loading, the effect of bulk diffusivity on τ_{eq} is slightly lessened by the larger condensation sink. Figure S1 shows the contour plots of τ_{eq} calculated using the analytical solution

https://doi.org/10.5194/egusphere-2026-4764
Preprint. Discussion started: 27 August 2026

to partitioning and reproduces very similar predicted τ_{eq} as the numerical solution in Fig. 2. Using the average case of $C_{OA} \sim 1$ μg m^{-3}, τ_{eq} is shorter than or equal to 20 min for all C^0 when $D_b \geq 10^{-15}$ cm^2 s^{-1}; therefore, we can apply the instantaneous equilibrium solution for particles with little bulk diffusion limitations (demarked in green) (Fig. 3b). In this equilibrium regime, τ_{eq} exhibits sensitivity to C^0 where lower C^0 corresponds to a prolonged τ_{eq} as more mass transfer must occur to reach equilibrium conditions. In more pristine conditions where the background aerosol concentrations are lower, *i.e.* $C_{OA} < 1$ μg m^{-3}, and τ_{eq} is greater than 20 minutes when $D_b > 10^{-15}$ cm^2 s^{-1} then there may be slight overestimation in the partitioned mass however this is not expected to be large as the aerosol burden in these areas would be minimal.

When particles are highly viscous with $D_b < 10^{-15}$ cm^2 s^{-1}, kinetic partitioning needs to be applied. The analytical solution (Fig. S1) is an adequate representation of partitioning behavior as benchmarked by the numerical solution (Fig. 2b); thus, partitioning can be approximated by Eq. (12) where the instantaneous analytical solution can be applied at $D_b < 10^{-15}$ cm^2 s^{-1}. For integration into GEOS-Chem, additional internal time stepping for partitioning may be undesirable as only the partitioned mass is needed at the end of the chemical time step. Figure S2 shows a contour plot of the final (t = 20 min) particle-phase concentration which is calculated through two approaches: (1) the numerical and analytical solutions with internal time stepping and (2) the instantaneous analytical solution without time stepping and without iteratively recalculating C_{OA} and k_{gp}. For the three tested mass loadings, when $D_b < 10^{-15}$ cm^2 s^{-1} the instantaneous analytical solution exhibits a linear trend that coincides with the linear portion of the numerical (and analytical) solution contour. Thus, when $D_b < 10^{-15}$ cm^2 s^{-1}, the instantaneous analytical solution can be used to accurately simulate the final particle-phase (and gas-phase) concentration at 20 minutes.

With the assumption that the average background aerosol concentration is within the magnitude of $C_{OA} = 1$ μg m^{-3}, we have implemented the algorithm as summarized: (1) if $D_b \geq 10^{-15}$ cm^2 s^{-1}, equilibrium partitioning is applied or (2) if $D_b < 10^{-15}$ cm^2 s^{-1}, then the instantaneous analytical solution is applied. We term this kinetic partitioning implementation as the "α_{eff} scheme" to replace the instantaneous equilibrium gas-particle partitioning scheme ("base" case) in GEOS-Chem.

https://doi.org/10.5194/egusphere-2026-4764
Preprint. Discussion started: 27 August 2026

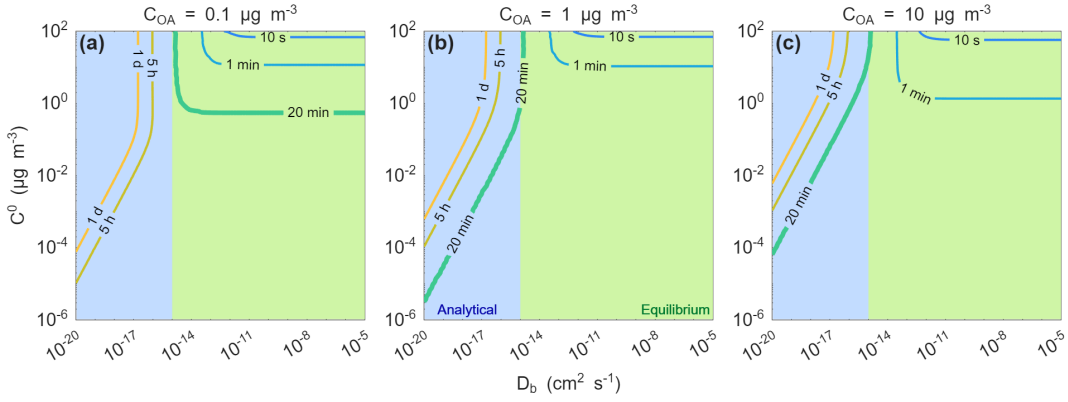

Figure 2. Contour plot of equilibration timescale (τ_{eq}) calculated using the numerical solution as a function of bulk diffusivity (D_b), saturation mass concentration (C^0), and initial pre-existing particle concentrations (C_{OA}) of **(a)** 0.1 μg m^{-3}, **(b)** 1 μg m^{-3}, and **(c)** 10 μg m^{-3}. The τ_{eq} is calculated using the numerical solution. Two colored regimes are depicted: (1) when $D_b \geq 10^{-15}$ cm^2 s^{-1}, equilibrium partitioning is applied (in green) and (2) if $D_b < 10^{-15}$ cm^2 s^{-1}, then the instantaneous analytical solution is applicable (in blue). The initial gas-phase concentration was 0.1 μg m^{-3} (to simulate condensation), or the initial particle-phase concentration was 0.1 μg m^{-3} (to simulate evaporation), and the temperature was set to 298K.

3.2 Global SOA Budget Simulations

In this section, we explore the effects of kinetic partitioning on simulated global SOA budgets. We implemented the α_{eff} kinetic partitioning scheme to simulate the two sets of TSOA and ASOA species. As we have incorporated the volatility-dependent ΔH_{vap} parameterization into our methods, to accurately visualize the change due to purely partitioning scheme differences, the "base" simulation includes effects due to the change in ΔH_{vap} calculation. This is because the assumption of ΔH_{vap} in combination with the initial gas-phase concentration modulates the potential aerosol formation (or evaporation) upon cooling (heating) (Fig. S3) (Cappa & Jimenez, 2010). Lower volatility species, *e.g.* C^0 = 0.1 μg m^{-3}, will have a higher heat of vaporization corresponding to a stronger temperature dependence therefore cooling enhances their preference for the particle phase compared to higher volatility compounds. Overall, the update to volatility-

https://doi.org/10.5194/egusphere-2026-4764
Preprint. Discussion started: 27 August 2026

dependent ΔH_{vap} resulted in global SOA burden increase driven by increased SOA concentrations especially in lower temperatures (Fig. S3).

Figure 3 presents the annually averaged D_b in SOA particles (using the α_{eff} scheme in GEOS-Chem) from the surface (vertical level 1), and two elevated hybrid-coordinate model altitudes (vertical levels 11 and 23). GEOS-Chem's hybrid sigma-pressure grid is terrain-following rather than being constant-pressure surfaces or fixed altitudes. Vertical levels 11 and 23 were selected as to representative tropospheric model levels which correspond to 850 hPa (above the boundary layer) and 500 hPa (in the free troposphere) for a column at atmospheric sea level (GEOS-Chem, 2026). Primarily at the surface level, SOA particles have typically $D_b \geq 10^{-10}$ cm^2 s^{-1}, indicating liquid-like particles with little kinetic limitations to partitioning. Western US, northern Africa, and the Tibetan Plateau are predicted to have slightly lower D_b representative of semisolid particles. Above the standard 850 hPa layer in these regions, lower D_b becomes more predominant at higher altitudes. At 500 hPa, D_b is expected to be mostly smaller than ~10^{-15} cm^2 s^{-1} in highly viscous particles apart from equatorial continents such as northern South America, sub-Saharan Africa, and Southeast Asia where SOA particles are less viscous with higher D_b. The spatial distribution of D_b agrees well with previous phase state predictions for large-scale models (Luu et al., 2025; Shiraiwa et al., 2017).

https://doi.org/10.5194/egusphere-2026-4764
Preprint. Discussion started: 27 August 2026

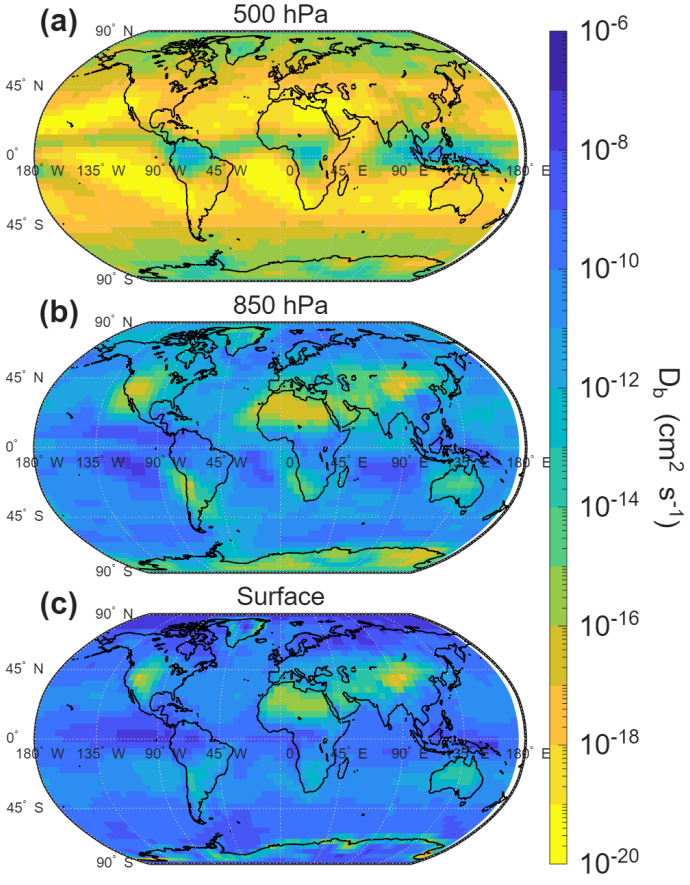

Figure 3. Simulated annually averaged bulk diffusivities (D_b) in SOA particles at selected representative tropospheric model levels which correspond to **(a)** 500 hPa and **(b)** 850 hPa for a column at atmospheric sea level. While **(c)** at the surface, corresponds to the true fixed terrain-following pressure surface.

Figure 4 shows the percent difference between annually predicted SOA budget with the α_{eff} kinetic partitioning scheme (see actual SOA mass loadings in Fig. S4) compared to the base case (Fig. S5). At the surface level, both schemes predict very similar concentrations, showing little-to-no changes in most regions. The α_{eff} scheme predicts up to 10% less mass over the western and central US due to kinetically limited condensational growth on viscous particles (Fig. 3c). Northern Africa and Tibetan Plateau are predicted to have roughly 20% higher SOA mass with the α_{eff}

https://doi.org/10.5194/egusphere-2026-4764
Preprint. Discussion started: 27 August 2026

scheme due to kinetic limitations to evaporation as low C_{OA} and high temperature conditions drive net evaporation in these regions. At 850 hPa, western US is predicted to have up to 10% less SOA mass predicted by the α_{eff} scheme, while offshore is predicted to have roughly 20% more SOA mass. Other regions such as off the coasts of Northwestern Africa, South Africa, and Chile are also predicted to have increased SOA mass up to 40%.

At 500 hPa, the effects of kinetic limitations on partitioning become significant, reaching upwards of 50% greater predicted SOA mass along the equatorial and mid-latitudes as evaporation is suppressed for glassy particles. Over the remote oceans (Indian and Pacific Oceans) and central US, we predict up to an order of magnitude SOA budget increase in the upper troposphere (Fig. S4a and S5a). This occurrence may be driven by the Hadley cell in the region that lifts SOA and its precursors to the tropical tropopause, particularly in the tropical rainforest regions in the Amazon, Congo, and Oceania. These continental detainment regions are more humid than elsewhere in the tropical upper troposphere and hence have higher D_b values (Fig. 3a) allowing SOA formation in cold temperatures. As the tropical tropopause air undergoes subsidence in the Hadley cell, the temperature increases, which drives evaporation; however, the RH simultaneously decreases, which lowers D_b more than the increasing temperature increases D_b (Fig. S6). Hence, the descending regions of the Hadley cell in the subtropics have $D_b < 10^{-16}$ cm^2 s^{-1}. While the warming temperatures drive evaporation in the base simulations, the low D_b values greatly delay evaporation with the α_{eff} scheme, leading to higher concentrations in this simulation. This is expected as solid particles are more prevalent under free troposphere conditions (low average temperatures and low C_{OA}) throughout the year (Fig. 3 and S4). During each season at 500 hPa, the predicted SOA mass difference trend prevails because of kinetic limitations on evaporation when $D_b < 10^{-16}$ cm^2 s^{-1} (Fig. S7). The suppression of evaporation is more prominent for higher volatility compounds with C^*(298 K) = 10 and 100 μg m^{-3} with up to 50% higher mass predicted with the α_{eff} scheme for a majority of the mid- to equatorial latitudes (Fig. S8). The annual lower troposphere averaging approximately 1% increase while the upper troposphere is about 15% increase in the SOA budget (Table S2).

https://doi.org/10.5194/egusphere-2026-4764
Preprint. Discussion started: 27 August 2026

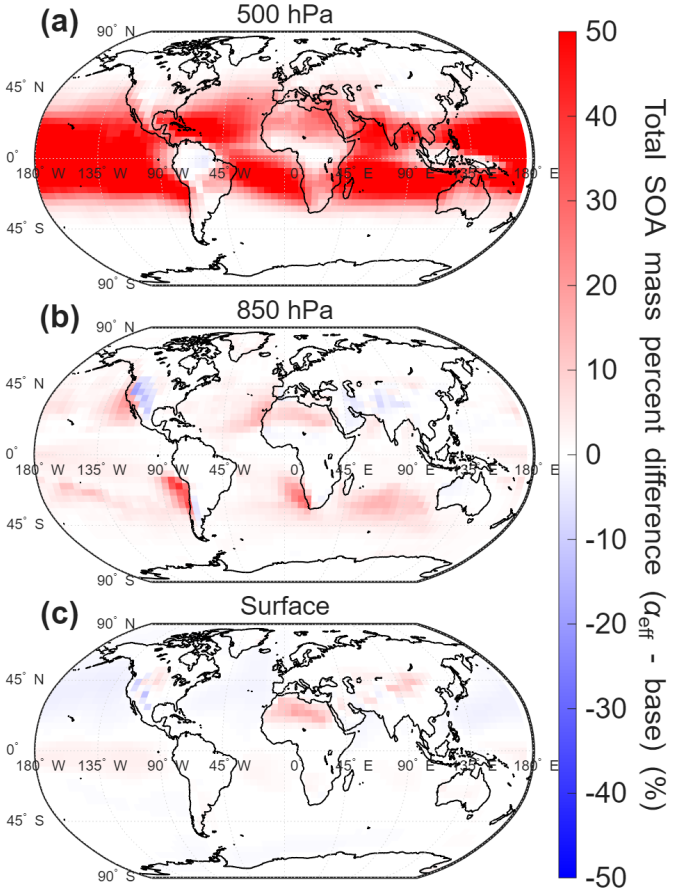

Figure 4. Predicted annual percent SOA mass loading differences **(a)** at the free troposphere, **(b)** above the boundary layer, and **(c)** at the surface between the α_{eff} kinetic and base case partitioning scheme simulations.

We show the seasonality of the SOA budget percent differences at the surface in Figure 5. In Northern hemisphere winter, the α_{eff} kinetic partitioning scheme predicts roughly a 40% decrease in SOA mass in the Western US but an approximately 30% increase in Saharan Africa (Fig. 5a). As for spring, there is a mixture of an increase in predicted SOA mass in Northern Great Plains of the US extending into Canada with a small decrease for Southwestern US (Fig. 5b). There is also up to a 50% increase in SOA budget in Saharan Africa and as much as 40% in the Tibetan Plateau. With increased average surface temperatures in the summer months, there are virtually no

https://doi.org/10.5194/egusphere-2026-4764
Preprint. Discussion started: 27 August 2026

401 differences in predicted SOA mass apart from the Tibetan Plateau as the equilibrium partitioning
402 assumption is valid when $D_b > 10^{-15}$ cm^2 s^{-1} (Fig. S9c). The following autumn months show a
403 mixture of enhancement and reduction in the SOA budget in western US and a slight increase
404 across Saharan Africa, Central Asia, and the Tibetan Plateau. From these plots, we observe that
405 each season demonstrates distinct spatial patterns of SOA budget discrepancies when kinetic
406 limitations are applied to the partitioning scheme. It is projected that on a finer temporal resolution
407 on the span of weeks or days, typically simulated for field campaign comparisons, weather
408 variability may make these predicted differences more significant, yet this remains to be further
409 investigated.

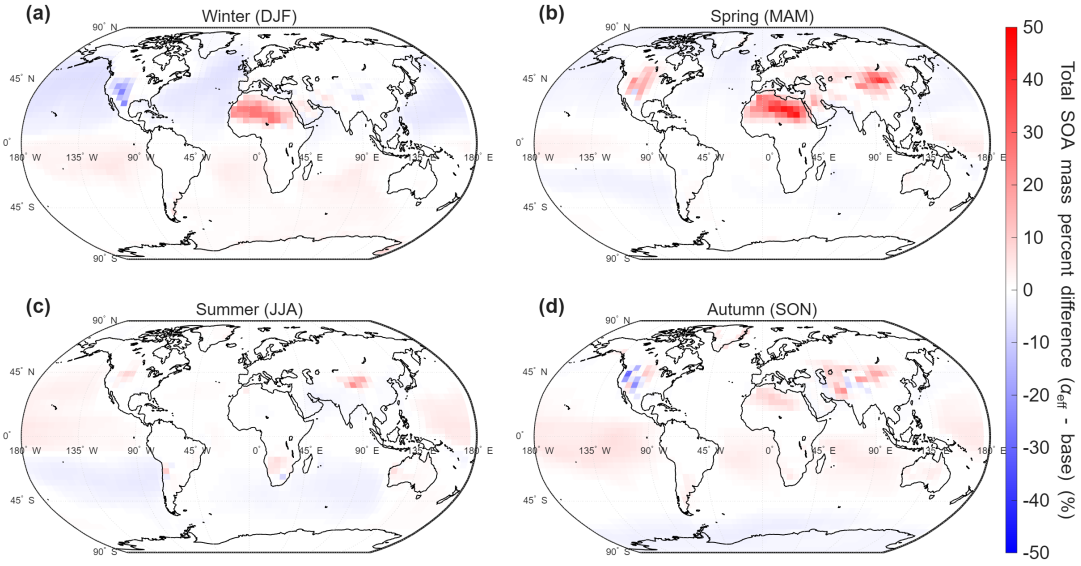

410

411 **Figure 5.** Predicted seasonal variations in percent SOA budget differences at the surface, during
412 Northern hemisphere **(a)** winter (Dec-Jan-Feb), **(b)** spring (Mar-Apr-May), **(c)** summer (Jun-Jul-
413 Aug), and **(d)** autumn (Sep-Oct-Nov).

414

415 **4 Method Limitations and Future Needs**

416 We address limitations in our methods and future needs. In the complex scheme,
417 oxygenated primary organic aerosol (OPOA) is formed through OH oxidation of emitted primary
418 organic gases (EPOG), producing oxidized primary organic gases (OPOG) that reversibly partition

https://doi.org/10.5194/egusphere-2026-4764
Preprint. Discussion started: 27 August 2026

into OPOA (Pai et al., 2020). Therefore, previous studies aimed at quantifying simulated OA burden have categorized OPOA differently either as POA (Pai et al., 2020; Pye & Seinfeld, 2010) or SOA (Brewer et al., 2023; Murphy et al., 2014). In this study, we have chosen to omit OPOA from our main SOA phase state calculations, as only two volatility bins each are used to represent both EPOG and their oxidation products, OPOA, which may not be sufficient constraints especially for phase state predictions which have been validated for SOA (DeRieux et al., 2018; Shiraiwa et al., 2014). Both POA and OPOA are considered for total organic aerosol mass concentration (C_{OA}) as the absorbing mass for partitioning as in the base scheme. Additionally, potential phase state impact on isoprene-derived SOA (ISOA) is not resolved in the present work. ISOA is not treated as a reversibly partitioning species but treated as non-reversible reactive uptake in GEOS-Chem. Further development is needed to include kinetic limitations to the reactive uptake of ISOA.

In the current GEOS-Chem configuration, SOA particles are implicitly assumed to be externally mixed from inorganic compounds or phase-separated, if internally mixed, with the predicted phase state representing only the organic phase. Phase separation could occur between SOA and POA (Huang et al., 2021), but they are treated as ideally well-mixed as both SOA and POA are included for the total absorbing mass (C_{OA}). We partially account for phase separation in the present work, by determining using SOA phase state to determine absorptive partitioning dynamics of all species. However, the effect of non-ideality determining phase separation or well-mixed bulk phase on SOA partitioning should be implemented in future studies, as has been explored in several studies (Schmedding et al., 2020; Serrano Damha et al., 2025). Additionally, SOA evaporation and heterogeneous chemistry can lead to the formation of a surface crust that may hinder further evaporation (Schervish et al., 2026; Zhou et al., 2019). Such complex effects should be further explored for potential treatments in CTMs in future studies.

α_{eff} is particle size dependent as α_{eff} is inversely related to D_p, whereas we assumed D_p = 100 nm in this study. The lack of particle size resolution with the GEOS-Chem complex scheme limits our results to one particle size, but GEOS-Chem-TOMAS' size tracking capabilities presents a potential for further investigation on the size-dependent kinetic limitations effects on the SOA budget. Note that recently a size-dependent α_{eff} has been implemented in GEOS-Chem-TOMAS to portion the SOA mass accordingly across size distribution, without altering the SOA budget

https://doi.org/10.5194/egusphere-2026-4764
Preprint. Discussion started: 27 August 2026

(O'Donnell et al., 2025). This development, though not impacting the total partitioning mass, should be included in further advancements in implementation of kinetic partitioning in GEOS-Chem-TOMAS.

5 Conclusions

In summary, we developed a computationally efficient method to simulate SOA phase state and its impacts on kinetic partitioning utilizing the effective mass accommodation coefficient in GEOS-Chem. This method effectively treats the effect of gas diffusion (i.e. condensation sink) as well as phase state and associated kinetic limitations on partitioning. We note that τ_{mix} represents kinetic limitations of bulk diffusion within SOA particles; however, τ_{mix} is not an accurate representation to describe SOA partitioning in aerosol modeling. A recent study by Li et al. (2026) implemented a phase-state dependent partitioning scheme using τ_{mix} as partitioning timescale; however, the use of τ_{mix} as an equilibration timescale of partitioning is fundamentally incorrect, leading to inaccurate representation of phase state impacts on SOA, as it ignores the effects of gas diffusion, volatility, and mass loadings on partitioning timescale, as discussed in detail in the box modeling section.

With implementation of α_{eff}-kinetic partitioning scheme in GEOS-Chem, we predict that SOA particles adopt viscous semisolid and glassy phase states in arid regions below the boundary layer and is the dominant phase state in the upper troposphere. We simulate that the kinetic limitations of SOA partitioning can lead to annual SOA mass deviation up to 50% for mid- to equatorial latitudes compared to instantaneous equilibrium partitioning above 500 hPa. Overall, we predict annually generally little change at the surface and at 850 hPa but significant perturbation in predicted SOA mass in dry regions and in the free troposphere. We anticipate stronger deviations for finer temporal resolution simulations as we expect a reduced dilution effect on the mass difference between the α_{eff} and base case with shorter time averaging. The development of this α_{eff} kinetic partitioning scheme enables comparison with aircraft observations to quantify impacts of SOA phase state in future studies. Observations of SOA mass loading in the upper troposphere would be especially compelling to investigate as predictions of high-altitude new particle formation may be improved from implementing the α_{eff} scheme for SOA partitioning. Addressing

https://doi.org/10.5194/egusphere-2026-4764
Preprint. Discussion started: 27 August 2026

this well-known knowledge gap may help achieve closure between SOA model simulations and field observations.

Code and Data Availability. The GEOS-Chem model is maintained by the Harvard Atmospheric Chemistry Modelling Group and the specific version (ver. 14.1.1) used in this work is permanently archived at https://doi.org/10.5281/zenodo.7696632 (Yantosca et al., 2023). The modified carbon_mod.f90 used in this work and the 0-D box model are archived at https://doi.org/10.5281/zenodo.22099483 (Luu et al., 2026). GEOS-Chem simulation outputs are available by contacting the corresponding author.

Author Contributions. RL, MSc, JP and MSh designed the research. RL developed the box model, GEOS-Chem implementation, and ran the simulations. RL and MSc conducted data analysis and all authors were involved in discussions. RL drafted the manuscript, MSh edited the manuscript, and all authors reviewed and commented on the paper.

Supplement. The supplement related to this article is available online.

Competing interests. We declare no competing interests.

Acknowledgments. This work was funded by the U.S. National Science Foundation (AGS-2246502).

References

Brewer, J. F., Jacob, D. J., Jathar, S. H., He, Y., Akherati, A., Zhai, S., Jo, D. S., Hodzic, A., Nault, B. A., Campuzano-Jost, P., Jimenez, J. L., Park, R. J., Oak, Y. J., & Liao, H. (2023). A Scheme for Representing Aromatic Secondary Organic Aerosols in Chemical Transport Models: Application to Source Attribution of Organic Aerosols Over South Korea During the KORUS-AQ Campaign. *Journal of Geophysical Research: Atmospheres*, *128*(8), e2022JD037257. https://doi.org/10.1029/2022JD037257

Cappa, C. D., & Jimenez, J. L. (2010). Quantitative estimates of the volatility of ambient organic aerosol. *Atmospheric Chemistry and Physics*, *10*(12), 5409–5424. https://doi.org/10.5194/acp-10-5409-2010

Chung, S. H., & Seinfeld, J. H. (2002). Global distribution and climate forcing of carbonaceous aerosols. *Journal of Geophysical Research: Atmospheres*, *107*(D19). https://doi.org/10.1029/2001jd001397

https://doi.org/10.5194/egusphere-2026-4764
Preprint. Discussion started: 27 August 2026

Community, T. I. G.-C. U. (2024a). *geos-chem/GeosCore/carbon_mod.F90*. In https://github.com/geoschem/geos-chem/blob/20e2402baf56c682cc04af74adb139efdb6ca000/GeosCore/carbon_mod.F90

Community, T. I. G.-C. U. (2024b). *geoschem/GCClassic: GCClassic 14.4.1*. In Zenodo. https://zenodo.org/records/12584192

D'Andrea, S. D., Häkkinen, S. A. K., Westervelt, D. M., Kuang, C., Levin, E. J. T., Kanawade, V. P., Leaitch, W. R., Spracklen, D. V., Riipinen, I., & Pierce, J. R. (2013). Understanding global secondary organic aerosol amount and size-resolved condensational behavior. *Atmospheric Chemistry and Physics*, *13*(22), 11519–11534. https://doi.org/10.5194/acp-13-11519-2013

DeRieux, W.-S. W., Li, Y., Lin, P., Laskin, J., Laskin, A., Bertram, A. K., Nizkorodov, S. A., & Shiraiwa, M. (2018). Predicting the glass transition temperature and viscosity of secondary organic material using molecular composition. *Atmospheric Chemistry and Physics*, *18*(9), 6331–6351. https://doi.org/10.5194/acp-18-6331-2018

Fisher, J. A., Jacob, D. J., Travis, K. R., Kim, P. S., Marais, E. A., Chan Miller, C., Yu, K., Zhu, L., Yantosca, R. M., Sulprizio, M. P., Mao, J., Wennberg, P. O., Crounse, J. D., Teng, A. P., Nguyen, T. B., St. Clair, J. M., Cohen, R. C., Romer, P., Nault, B. A.,…Mikoviny, T. (2016). Organic nitrate chemistry and its implications for nitrogen budgets in an isoprene- and monoterpene-rich atmosphere: constraints from aircraft (SEAC⁴RS) and ground-based (SOAS) observations in the Southeast US. *Atmospheric Chemistry and Physics*, *16*(9), 5969–5991. https://doi.org/10.5194/acp-16-5969-2016

GEOS-Chem. (2026). *GEOS-Chem Classic vertical grids*. https://geos-chem.readthedocs.io/en/latest/supplemental-guides/vertical-grids.html

Hallquist, M., Wenger, J. C., Baltensperger, U., Rudich, Y., Simpson, D., Claeys, M., Dommen, J., Donahue, N. M., George, C., Goldstein, A. H., Hamilton, J. F., Herrmann, H., Hoffmann, T., Iinuma, Y., Jang, M., Jenkin, M. E., Jimenez, J. L., Kiendler-Scharr, A., Maenhaut, W.,…Wildt, J. (2009). The formation, properties and impact of secondary organic aerosol: current and emerging issues. *Atmospheric Chemistry and Physics*, *9*(14), 5155–5236. https://doi.org/10.5194/acp-9-5155-2009

He, Y., Bilsback, K. R., Shrivastava, M., Zaveri, R. A., Shilling, J. E., Seinfeld, J. H., Zhao, B., Wang, S., Cappa, C. D., Pierce, J. R., & Jathar, S. H. (2025). Kinetic Modeling of Secondary Organic Aerosol in a Weather-Chemistry Model: Parameterizations, Processes, and Predictions for GOAmazon. *ACS ES&T Air*, *2*(2), 249–263. https://doi.org/10.1021/acsestair.4c00240

Hindmarsh, A. C. (1983). ODEPACK, A Systematized Collection of ODE Solvers. *Scientific Computing*, *1*(IMACS Transactions), 55–64.

Hodzic, A., Kasibhatla, P. S., Jo, D. S., Cappa, C. D., Jimenez, J. L., Madronich, S., & Park, R. J. (2016). Rethinking the global secondary organic aerosol (SOA) budget: stronger production, faster removal, shorter lifetime. *Atmospheric Chemistry and Physics*, *16*(12), 7917–7941. https://doi.org/10.5194/acp-16-7917-2016

Huang, Y., Mahrt, F., Xu, S., Shiraiwa, M., Zuend, A., & Bertram, A. K. (2021). Coexistence of three liquid phases in individual atmospheric aerosol particles. *Proceedings of the National Academy of Sciences*, *118*(16), e2102512118. https://doi.org/doi:10.1073/pnas.2102512118

https://doi.org/10.5194/egusphere-2026-4764
Preprint. Discussion started: 27 August 2026

Jensen, L. N., Kristensen, K., Iversen, E. M., Canagaratna, M. R., Roldin, P., & Bilde, M. (2025). Nature of Temperature-Induced Phase Transitions in Secondary Organic Aerosol Particles. *Environmental Science & Technology*, *59*(45), 24359–24367. https://doi.org/10.1021/acs.est.5c08582

Jimenez, J. L., Canagaratna, M. R., Donahue, N. M., Prevot, A. S. H., Zhang, Q., Kroll, J. H., DeCarlo, P. F., Allan, J. D., Coe, H., Ng, N. L., Aiken, A. C., Docherty, K. S., Ulbrich, I. M., Grieshop, A. P., Robinson, A. L., Duplissy, J., Smith, J. D., Wilson, K. R., Lanz, V. A.,…Worsnop, D. R. (2009). Evolution of Organic Aerosols in the Atmosphere. *Science*, *326*(5959), 1525–1529. https://doi.org/doi:10.1126/science.1180353

Julin, J., Winkler, P. M., Donahue, N. M., Wagner, P. E., & Riipinen, I. (2014). Near-Unity Mass Accommodation Coefficient of Organic Molecules of Varying Structure. *Environmental Science & Technology*, *48*(20), 12083–12089. https://doi.org/10.1021/es501816h

Kanakidou, M., Seinfeld, J. H., Pandis, S. N., Barnes, I., Dentener, F. J., Facchini, M. C., Van Dingenen, R., Ervens, B., Nenes, A., Nielsen, C. J., Swietlicki, E., Putaud, J. P., Balkanski, Y., Fuzzi, S., Horth, J., Moortgat, G. K., Winterhalter, R., Myhre, C. E. L., Tsigaridis, K.,…Wilson, J. (2005). Organic aerosol and global climate modelling: a review. *Atmospheric Chemistry and Physics*, *5*(4), 1053–1123. https://doi.org/10.5194/acp-5-1053-2005

Kirkby, J., Amorim, A., Baltensperger, U., Carslaw, K. S., Christoudias, T., Curtius, J., Donahue, N. M., Haddad, I. E., Flagan, R. C., Gordon, H., Hansel, A., Harder, H., Junninen, H., Kulmala, M., Kürten, A., Laaksonen, A., Lehtipalo, K., Lelieveld, J., Möhler, O.,…Worsnop, D. R. (2023). Atmospheric new particle formation from the CERN CLOUD experiment. *Nature Geoscience*, *16*(11), 948–957. https://doi.org/10.1038/s41561-023-01305-0

Koop, T., Bookhold, J., Shiraiwa, M., & Pöschl, U. (2011). Glass transition and phase state of organic compounds: dependency on molecular properties and implications for secondary organic aerosols in the atmosphere. *Physical Chemistry Chemical Physics*, *13*(43), 19238–19255. https://doi.org/10.1039/C1CP22617G

Kroll, J. H., & Seinfeld, J. H. (2008). Chemistry of secondary organic aerosol: Formation and evolution of low-volatility organics in the atmosphere. *Atmospheric Environment*, *42*(16), 3593–3624. https://doi.org/10.1016/j.atmosenv.2008.01.003

Li, Y., Day, D. A., Stark, H., Jimenez, J. L., & Shiraiwa, M. (2020). Predictions of the glass transition temperature and viscosity of organic aerosols from volatility distributions. *Atmospheric Chemistry and Physics*, *20*(13), 8103–8122. https://doi.org/10.5194/acp-20-8103-2020

Li, Y., Heald, C. L., Miao, R., Campuzano-Jost, P., & Jimenez, J. L. (2026). Global Impacts of Simulating Organic Aerosol Phase State. *Environmental Science & Technology*. https://doi.org/10.1021/acs.est.5c13238

Li, Y., & Shiraiwa, M. (2019). Timescales of secondary organic aerosols to reach equilibrium at various temperatures and relative humidities. *Atmospheric Chemistry and Physics*, *19*(9), 5959–5971. https://doi.org/10.5194/acp-19-5959-2019

Lin, H., Emmons, L. K., Lundgren, E. W., Yang, L. H., Feng, X., Dang, R., Zhai, S., Tang, Y., Kelp, M. M., Colombi, N. K., Eastham, S. D., Fritz, T. M., & Jacob, D. J. (2024). Intercomparison of GEOS-Chem and CAM-chem tropospheric oxidant chemistry within the Community Earth System Model version 2 (CESM2). *Atmospheric Chemistry and Physics*, *24*(15), 8607–8624. https://doi.org/10.5194/acp-24-8607-2024

https://doi.org/10.5194/egusphere-2026-4764
Preprint. Discussion started: 27 August 2026

Liu, X., Day, D. A., Krechmer, J. E., Brown, W., Peng, Z., Ziemann, P. J., & Jimenez, J. L. (2019). Direct measurements of semi-volatile organic compound dynamics show near-unity mass accommodation coefficients for diverse aerosols. *Communications Chemistry*, *2*(1), 98. https://doi.org/10.1038/s42004-019-0200-x

Luu, R., Schervish, M., June, N. A., O'Donnell, S. E., Jathar, S. H., Pierce, J. R., & Shiraiwa, M. (2025). Global Simulations of Phase State and Equilibration Time Scales of Secondary Organic Aerosols with GEOS-Chem. *ACS Earth and Space Chemistry*, *9*(2), 288–302. https://doi.org/10.1021/acsearthspacechem.4c00281

Luu, R., Schervish, M., O'Donnell, E. S., Pierce, R. J., & Shiraiwa, M. (2026). *carbon_mod - added aeff kinetic partitioning scheme* In (Version v1.0.0-alpha) https://doi.org/10.5281/zenodo.22099483

Maclean, A. M., Butenhoff, C. L., Grayson, J. W., Barsanti, K., Jimenez, J. L., & Bertram, A. K. (2017). Mixing times of organic molecules within secondary organic aerosol particles: a global planetary boundary layer perspective. *Atmospheric Chemistry and Physics*, *17*(21), 13037–13048. https://doi.org/10.5194/acp-17-13037-2017

Marais, E. A., Jacob, D. J., Jimenez, J. L., Campuzano-Jost, P., Day, D. A., Hu, W., Krechmer, J., Zhu, L., Kim, P. S., Miller, C. C., Fisher, J. A., Travis, K., Yu, K., Hanisco, T. F., Wolfe, G. M., Arkinson, H. L., Pye, H. O. T., Froyd, K. D., Liao, J., & McNeill, V. F. (2016). Aqueous-phase mechanism for secondary organic aerosol formation from isoprene: application to the southeast United States and co-benefit of SO₂ emission controls. *Atmospheric Chemistry and Physics*, *16*(3), 1603–1618. https://doi.org/10.5194/acp-16-1603-2016

Murphy, B. N., Donahue, N. M., Robinson, A. L., & Pandis, S. N. (2014). A naming convention for atmospheric organic aerosol. *Atmospheric Chemistry and Physics*, *14*(11), 5825–5839. https://doi.org/10.5194/acp-14-5825-2014

O'Brien, R. E., Neu, A., Epstein, S. A., MacMillan, A. C., Wang, B., Kelly, S. T., Nizkorodov, S. A., Laskin, A., Moffet, R. C., & Gilles, M. K. (2014). Physical properties of ambient and laboratory-generated secondary organic aerosol. *Geophysical Research Letters*, *41*(12), 4347–4353. https://doi.org/10.1002/2014GL060219

O'Donnell, S. E., Croft, B., Ford, B., June, N. A., Kuang, C., Singh, A., Chang, R. Y.-W., Collins, D. R., Hakala, S., Jathar, S. H., Paasonen, P., Shrivastava, M., Smith, J. N., & Pierce, J. R. (2025). Going Off Grid: A Comparative Study of the Lagrangian and Eulerian Perspectives of New Particle Formation Events. *Journal of Geophysical Research: Atmospheres*, *130*(18), e2025JD043713. https://doi.org/https://doi.org/10.1029/2025JD043713

Pai, S. J., Heald, C. L., Pierce, J. R., Farina, S. C., Marais, E. A., Jimenez, J. L., Campuzano-Jost, P., Nault, B. A., Middlebrook, A. M., Coe, H., Shilling, J. E., Bahreini, R., Dingle, J. H., & Vu, K. (2020). An evaluation of global organic aerosol schemes using airborne observations. *Atmospheric Chemistry and Physics*, *20*(5), 2637–2665. https://doi.org/10.5194/acp-20-2637-2020

Pankow, J. F. (1994). An absorption model of gas-particle partitioning of organic-compounds in the atmosphere. *Atmospheric Environment*, *28*(2), 185–188.

Pankow, J. F. (2003). Gas/particle partitioning of neutral and ionizing compounds to single and multi-phase aerosol particles. 1. Unified modeling framework. *Atmospheric Environment*, *37*(24), 3323–3333. https://doi.org/https://doi.org/10.1016/S1352-2310(03)00346-7

https://doi.org/10.5194/egusphere-2026-4764
Preprint. Discussion started: 27 August 2026

Pierce, J. R., & Adams, P. J. (2009). Uncertainty in global CCN concentrations from uncertain aerosol nucleation and primary emission rates. *Atmospheric Chemistry and Physics*, *9*(4), 1339–1356. https://doi.org/10.5194/acp-9-1339-2009

Pöschl, U., Rudich, Y., & Ammann, M. (2007). Kinetic model framework for aerosol and cloud surface chemistry and gas-particle interactions – Part 1: General equations, parameters, and terminology. *Atmospheric Chemistry and Physics*, *7*(23), 5989–6023. https://doi.org/10.5194/acp-7-5989-2007

Pöschl, U., & Shiraiwa, M. (2015). Multiphase Chemistry at the Atmosphere–Biosphere Interface Influencing Climate and Public Health in the Anthropocene. *Chemical Reviews*, *115*(10), 4440–4475. https://doi.org/10.1021/cr500487s

Pye, H. O. T., Chan, A. W. H., Barkley, M. P., & Seinfeld, J. H. (2010). Global modeling of organic aerosol: the importance of reactive nitrogen (NO_x and NO₃). *Atmospheric Chemistry and Physics*, *10*(22), 11261–11276. https://doi.org/10.5194/acp-10-11261-2010

Pye, H. O. T., & Seinfeld, J. H. (2010). A global perspective on aerosol from low-volatility organic compounds. *Atmospheric Chemistry and Physics*, *10*(9), 4377–4401. https://doi.org/10.5194/acp-10-4377-2010

Reid, J. P., Bertram, A. K., Topping, D. O., Laskin, A., Martin, S. T., Petters, M. D., Pope, F. D., & Rovelli, G. (2018). The viscosity of atmospherically relevant organic particles. *Nature Communications*, *9*(1), 956. https://doi.org/10.1038/s41467-018-03027-z

Saukko, E., Lambe, A. T., Massoli, P., Koop, T., Wright, J. P., Croasdale, D. R., Pedernera, D. A., Onasch, T. B., Laaksonen, A., Davidovits, P., Worsnop, D. R., & Virtanen, A. (2012). Humidity-dependent phase state of SOA particles from biogenic and anthropogenic precursors. *Atmospheric Chemistry and Physics*, *12*(16), 7517–7529. https://doi.org/10.5194/acp-12-7517-2012

Schervish, M., Donahue, N. M., & Shiraiwa, M. (2024). Effects of volatility, viscosity, and non-ideality on particle–particle mixing timescales of secondary organic aerosols. *Aerosol Science and Technology*, *58*(4), 411–426. https://doi.org/10.1080/02786826.2023.2256827

Schervish, M., Kang, H. G., Wingen, L. M., Nguyen, K., Begay, C., Wilson, J., Shrivastava, M., Chen, Y., Shilling, J. E., Ng, N. L., Pöschl, U., Berkemeier, T., Zelenyuk, A., & Shiraiwa, M. (2026). Surface Crust Formation Controls Evaporation Kinetics of Secondary Organic Aerosols. *Environmental Science & Technology*, *60*(10), 7995–8006. https://doi.org/10.1021/acs.est.5c11018

Schervish, M., & Shiraiwa, M. (2023). Impact of phase state and non-ideal mixing on equilibration timescales of secondary organic aerosol partitioning. *Atmospheric Chemistry and Physics*, *23*(1), 221–233. https://doi.org/10.5194/acp-23-221-2023

Schmedding, R., Rasool, Q. Z., Zhang, Y., Pye, H. O. T., Zhang, H., Chen, Y., Surratt, J. D., Lopez-Hilfiker, F. D., Thornton, J. A., Goldstein, A. H., & Vizuete, W. (2020). Predicting secondary organic aerosol phase state and viscosity and its effect on multiphase chemistry in a regional-scale air quality model. *Atmospheric Chemistry and Physics*, *20*(13), 8201–8225. https://doi.org/10.5194/acp-20-8201-2020

Seinfeld, J. H., & Pandis, S. N. (2016). *Atmospheric Chemistry and Physics: From Air Pollution to Climate Change* (3rd ed.). Wiley.

Serrano Damha, C., Gorkowski, K., & Zuend, A. (2025). Implications of reduced-complexity aerosol thermodynamics on organic aerosol mass concentration and composition over

https://doi.org/10.5194/egusphere-2026-4764
Preprint. Discussion started: 27 August 2026

North America. *Atmos. Chem. Phys.*, *25*(11), 5773–5792. https://doi.org/10.5194/acp-25-5773-2025

Shiraiwa, M., Ammann, M., Koop, T., & Pöschl, U. (2011). Gas uptake and chemical aging of semisolid organic aerosol particles. *Proceedings of the National Academy of Sciences*, *108*(27), 11003–11008. https://doi.org/10.1073/pnas.1103045108

Shiraiwa, M., Berkemeier, T., Schilling-Fahnestock, K. A., Seinfeld, J. H., & Pöschl, U. (2014). Molecular corridors and kinetic regimes in the multiphase chemical evolution of secondary organic aerosol. *Atmospheric Chemistry and Physics*, *14*(16), 8323–8341. https://doi.org/10.5194/acp-14-8323-2014

Shiraiwa, M., Li, Y., Tsimpidi, A. P., Karydis, V. A., Berkemeier, T., Pandis, S. N., Lelieveld, J., Koop, T., & Pöschl, U. (2017). Global distribution of particle phase state in atmospheric secondary organic aerosols. *Nature Communications*, *8*(1), 15002. https://doi.org/10.1038/ncomms15002

Shiraiwa, M., Pfrang, C., Koop, T., & Pöschl, U. (2012). Kinetic multi-layer model of gas-particle interactions in aerosols and clouds (KM-GAP): linking condensation, evaporation and chemical reactions of organics, oxidants and water. *Atmospheric Chemistry and Physics*, *12*(5), 2777–2794. https://doi.org/10.5194/acp-12-2777-2012

Shiraiwa, M., & Pöschl, U. (2021). Mass accommodation and gas–particle partitioning in secondary organic aerosols: dependence on diffusivity, volatility, particle-phase reactions, and penetration depth. *Atmospheric Chemistry and Physics*, *21*(3), 1565–1580. https://doi.org/10.5194/acp-21-1565-2021

Shiraiwa, M., & Seinfeld, J. H. (2012). Equilibration timescale of atmospheric secondary organic aerosol partitioning. *Geophysical Research Letters*, *39*, L24801. https://doi.org/10.1029/2012GL054008

Shiraiwa, M., Zuend, A., Bertram, A. K., & Seinfeld, J. H. (2013). Gas-particle partitioning of atmospheric aerosols: interplay of physical state, non-ideal mixing and morphology [10.1039/C3CP51595H]. *Physical Chemistry Chemical Physics*, *15*(27), 11441–11453. https://doi.org/10.1039/C3CP51595H

Shrivastava, M., Cappa, C. D., Fan, J., Goldstein, A. H., Guenther, A. B., Jimenez, J. L., Kuang, C., Laskin, A., Martin, S. T., Ng, N. L., Petaja, T., Pierce, J. R., Rasch, P. J., Roldin, P., Seinfeld, J. H., Shilling, J., Smith, J. N., Thornton, J. A., Volkamer, R.,…Zhang, Q. (2017). Recent advances in understanding secondary organic aerosol: Implications for global climate forcing. *Reviews of Geophysics*, *55*(2), 509–559. https://doi.org/10.1002/2016RG000540

Shrivastava, M., Fan, J., Zhang, Y., Rasool, Q. Z., Zhao, B., Shen, J., Pierce, J. R., Jathar, S. H., Akherati, A., Zhang, J., Zaveri, R. A., Gaudet, B., Liu, Y., Andreae, M. O., Pöhlker, M. L., Donahue, N. M., Wang, Y., & Seinfeld, J. H. (2024). Intense formation of secondary ultrafine particles from Amazonian vegetation fires and their invigoration of deep clouds and precipitation. *One Earth*, *7*(6), 1029–1043. https://doi.org/10.1016/j.oneear.2024.05.015

Stolzenburg, D., Fischer, L., Vogel, A. L., Heinritzi, M., Schervish, M., Simon, M., Wagner, A. C., Dada, L., Ahonen, L. R., Amorim, A., Baccarini, A., Bauer, P. S., Baumgartner, B., Bergen, A., Bianchi, F., Breitenlechner, M., Brilke, S., Buenrostro Mazon, S., Chen, D.,…Winkler, P. M. (2018). Rapid growth of organic aerosol nanoparticles over a wide tropospheric temperature range. *Proceedings of the National Academy of Sciences*, *115*(37), 9122–9127. https://doi.org/10.1073/pnas.1807604115

https://doi.org/10.5194/egusphere-2026-4764
Preprint. Discussion started: 27 August 2026

Stolzenburg, D., Wang, M., Schervish, M., & Donahue, N. M. (2022). Tutorial: Dynamic organic growth modeling with a volatility basis set. *Journal of Aerosol Science*, *166*, 106063. https://doi.org/10.1016/j.jaerosci.2022.106063

Trump, E. R., Riipinen, I., & Donahue, N. M. (2014). Interactions between atmospheric ultrafine particles and secondary organic aerosol mass: a model study. *Boreal Environ. Res.*, *19*, 352–362.

Tsigaridis, K., Daskalakis, N., Kanakidou, M., Adams, P. J., Artaxo, P., Bahadur, R., Balkanski, Y., Bauer, S. E., Bellouin, N., Benedetti, A., Bergman, T., Berntsen, T. K., Beukes, J. P., Bian, H., Carslaw, K. S., Chin, M., Curci, G., Diehl, T., Easter, R. C.,…Zhang, X. (2014). The AeroCom evaluation and intercomparison of organic aerosol in global models. *Atmospheric Chemistry and Physics*, *14*(19), 10845–10895. https://doi.org/10.5194/acp-14-10845-2014

Vaden, T. D., Imre, D., Beránek, J., Shrivastava, M., & Zelenyuk, A. (2011). Evaporation kinetics and phase of laboratory and ambient secondary organic aerosol. *Proceedings of the National Academy of Sciences*, *108*(6), 2190–2195. https://doi.org/10.1073/pnas.1013391108

Virtanen, A., Joutsensaari, J., Koop, T., Kannosto, J., Yli-Pirilä, P., Leskinen, J., Mäkelä, J. M., Holopainen, J. K., Pöschl, U., Kulmala, M., Worsnop, D. R., & Laaksonen, A. (2010). An amorphous solid state of biogenic secondary organic aerosol particles. *Nature*, *467*(7317), 824–827. https://doi.org/10.1038/nature09455

Yantosca, B., Sulprizio, M., Lundgren, L., kelvinhb, Keller, C., Fritz, T., 22degrees, Ridley, D., Lin, H., Bindle, L., michael-s-long, Eastham, S. D., tsherwen, Downs, W., Fisher, J., Thackray, C., Holmes, C., GanLuo, Zhuang, J.,…Jourdan-He. (2023). *geoschem/geos-chem: GEOS-Chem 14.1.1*. In (Version 14.1.1)

Zaveri, R. A., Easter, R. C., Shilling, J. E., & Seinfeld, J. H. (2014). Modeling kinetic partitioning of secondary organic aerosol and size distribution dynamics: representing effects of volatility, phase state, and particle-phase reaction. *Atmospheric Chemistry and Physics*, *14*(10), 5153–5181. https://doi.org/10.5194/acp-14-5153-2014

Zaveri, R. A., Shilling, J. E., Zelenyuk, A., Zawadowicz, M. A., Suski, K., China, S., Bell, D. M., Veghte, D., & Laskin, A. (2020). Particle-Phase Diffusion Modulates Partitioning of Semivolatile Organic Compounds to Aged Secondary Organic Aerosol. *Environmental Science & Technology*, *54*(5), 2595–2605. https://doi.org/10.1021/acs.est.9b05514

Zhang, Z., Li, Y., Ran, H., An, J., Qu, Y., Zhou, W., Xu, W., Hu, W., Xie, H., Wang, Z., Sun, Y., & Shiraiwa, M. (2024). Simulated phase state and viscosity of secondary organic aerosols over China. *Atmospheric Chemistry and Physics*, *24*(8), 4809–4826. https://doi.org/10.5194/acp-24-4809-2024

Zhou, S., Hwang, B. C. H., Lakey, P. S. J., Zuend, A., Abbatt, J. P. D., & Shiraiwa, M. (2019). Multiphase reactivity of polycyclic aromatic hydrocarbons is driven by phase separation and diffusion limitations. *Proceedings of the National Academy of Sciences*, *116*(24), 11658–11663. https://doi.org/10.1073/pnas.1902517116